Spontaneous Imbibition in a Square Tube With Corner Films: Theoretical Model and Numerical Simulation

Zhao, Jianlin
Qin, Feifei
Fischer, Robert
Kang, Qinjun
Derome, Dominique
Carmeliet, Jan

To be published in: Water Resources Research

DOI to publisher's version: 10.1029/2020WR029190

Spontaneous imbibition in a square tube with corner films: theoretical model and numerical simulation

Jianlin Zhao[1], Feifei Qin[1], Robert Fischer[1,4,5], Qinjun Kang[3], Dominique Derome[2], Jan Carmeliet[1]

[1] Chair of Building Physics, Department of Mechanical and Process Engineering, ETH Zürich, 8092 Zürich, Switzerland

[2] Department of Civil and Building Engineering, Université de Sherbrooke, Sherbrooke Qc J1K 2R1, Canada

[3] Earth and Environmental Sciences Division, Los Alamos National Laboratory, Los Alamos, NM 87545, USA

[4] Laboratory for Multiscale Studies in Building Physics, Swiss Federal Laboratories for Materials Science and Technology, Empa, 8600 Dübendorf, Switzerland

[5] Laboratory for Biomimetic Membranes and Textiles, Swiss Federal Laboratories for Materials Science and Technology, Empa, 9014 St Gallen, Switzerland

Corresponding author: Jianlin Zhao (zhaojia@ethz.ch)

Key Points:

- A modified interacting capillary bundle is developed to describe imbibition in a square tube with corner film.
- Imbibition dynamics with corner film under various conditions are studied with both numerical and theoretical models.
- A universal scaling law of imbibition for the main meniscus is developed and the scaling law for arc meniscus is analyzed.

This is the author manuscript accepted for publication and has undergone full peer review but has not been through the copyediting, typesetting, pagination and proofreading process, which may lead to differences between this version and the Version of Record. Please cite this article as doi: 10.1029/2020WR029190.

Abstract

Spontaneous imbibition in an angular tube with corner films is a fundamental problem in many scientific and engineering processes. In this paper, a modified interacting capillary bundle model is developed to describe the liquid imbibition dynamics in a square tube with corner films. The square tube is decomposed into several interacting sub-capillaries and the local capillary pressure in each sub-capillary is derived based on the specific shape of its meniscus. The conductance of each sub-capillary is calculated using single-phase lattice Boltzmann simulation. The modified interacting capillary bundle model and color-gradient lattice Boltzmann method are used to simulate the liquid imbibition dynamics in the square tube with different fluid properties. The predictions by the modified interacting capillary bundle model match well with the lattice Boltzmann simulation results for different conditions, demonstrating the accuracy and robustness of the interacting capillary bundle model to describe the imbibition dynamics with corner films. In addition, the interacting capillary bundle model is helpful to investigate the mechanisms during spontaneous imbibition and the influences of fluid viscosity, surface tension, wetting phase contact angle and gravity on imbibition dynamics. Finally, a universal scaling law of imbibition dynamics for the main meniscus is developed and the scaling law for arc meniscus is also analyzed.

1 Introduction

Spontaneous imbibition, where a non-wetting fluid is displaced by a wetting fluid by capillary forces, in porous media is a common phenomenon encountered in many scientific and engineering processes (Li et al., 2019; Meng et al., 2017; Qin & van Brummelen, 2019; Schmid & Geiger, 2012), such as oil recovery (Morrow & Mason, 2001; Yang et al., 2019), filtration in soil (Kao & Hunt, 1996), wicking in textiles (Parada, Derome, et al., 2017; Parada, Vontobel, et al., 2017) or paper-like materials (Liu et al., 2018), etc. In order to analyze the underlying mechanisms of spontaneous imbibition, porous media are usually simplified such that they consist of regular shaped capillaries (Cai et al., 2014), including cylindrical and angular tubes. In studies of spontaneous imbibition, liquid-gas systems are usually considered and the pressure in the non-wetting phase, i.e. the gas phase, is assumed to be constant.

Spontaneous imbibition in a circular tube is governed by different forces such as the capillary, viscous, inertial and gravitational forces. In the different stages of the imbibition

process, different forces can override the uptake process. At the onset of the imbibition process, the viscous and gravitational forces can be neglected due to the quite small imbibition length, $h \to 0$. Therefore, imbibition is governed by the capillary and inertial forces, and this period is referred to as the inertial or inviscid regime (Das et al., 2012; De Gennes et al., 2013). Under this condition, the imbibition length (h) shows a linear relationship with time (t):

$$h = \sqrt{\frac{2\gamma\cos\theta}{\rho R}}t, \tag{1}$$

where γ is the surface tension, θ is the wetting phase contact angle, ρ is the liquid density, R is the inscribed radius of the tube. The time scale for the inertial regime is $t \sim \sqrt{\rho R^3/\gamma}$ (Das et al., 2012), which is usually quite short in comparison to the time scale of the whole imbibition process.

When the imbibition length becomes sufficiently long, the influence of inertial force can be neglected and this period is referred to as the viscous regime, which is governed by the capillary and viscous forces provided that the gravitational force can be neglected, for example imbibition in horizontal tubes or tubes with sufficiently small cross-section. Assuming Hagen–Poiseuille flow in the tube, the displacement of the main meniscus can be described by the well-known Washburn equation (Washburn, 1921):

$$h = \sqrt{\frac{\gamma\cos\theta R}{2\mu}t} \tag{2}$$

For liquid imbibition in a vertical tube, the gravitational force must be considered and the following equation describes the imbibition process (Washburn, 1921):

$$-h - \frac{2\gamma\cos\theta}{\rho g R}\ln\left(1 - \frac{\rho g R}{2\gamma\cos\theta}h\right) = \frac{\rho g R^2}{8\mu}t \tag{3}$$

The above equation has been further modified by Fries & Dreyer (2008a) in an explicit form. Between the inertial and viscous regimes lies the visco-inertial regime (Bosanquet, 1923), in which both the inertial and viscous forces have to be considered. The transition between different regimes for a circular tube has been studied by Fries & Dreyer (2008b).

In actual porous materials, the geometry of pores can be quite irregular (Yang et al., 2015). It is thus more representative to consider pores as angular tubes with corners, e.g. with square or triangular cross-sections, than circular tubes. Angular tubes are different from cylindrical tubes as corner films can develop along their edges (Wu et al., 2020). For a corner of a tube with half-angle of α, an arc meniscus can develop in this corner in front of the main meniscus if the wetting phase contact angle is smaller than (π/2-α), as shown in **Figure 1**. The imbibition dynamics of the main meniscus is similar to that in a circular tube due to the similar formats of driving and resistance forces (Gurumurthy et al., 2018), but the imbibition of the corner film is quite different because of the changing shapes of the arc meniscus along the corner. In addition, the corner flow of arc meniscus is coupled with the bulk flow of the main meniscus, making the imbibition process more complicated. Many efforts have been devoted to this specific liquid imbibition phenomenon and the scaling law between imbibition length (h) and time (t) for corner film has been investigated with different methods.

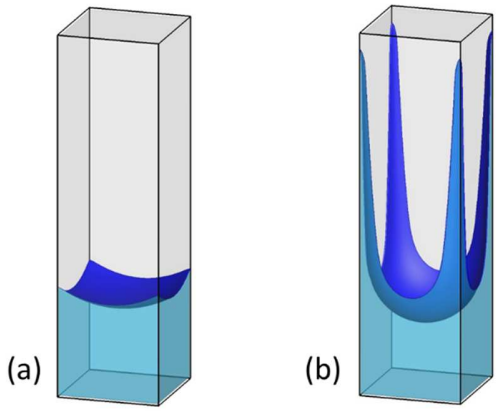

Figure 1. Wetting fluid distributions in a square tube under different contact angle. (a) θ=60°, (b) θ=12.6°.

Dong & Chatzis (1995) firstly analytically calculated the imbibition of corner film in a square tube without gravity effect and found that, for long imbibition time, the tip of the corner film moves as $h \propto t^{1/2}$. In addition, the influence of different parameters on imbibition in corner film was analyzed. Yu et al. (2018) analyzed the imbibition dynamics of both the main and the arc menisci with the least energy dissipation principle and found that both menisci move with $t^{1/2}$, but the uptake rates are described by different coefficients. Gravity was also not considered in their work. Weislogel (2012) used the Laplacian scaling method to describe the imbibition

dynamics of corner film and also obtained the scaling law of $h \propto t^{1/2}$ when no gravity effect was considered. When gravity was considered, assuming that the capillary pressure at the tip of the corner film is balanced with the hydrostatic head, the scaling law of $h \propto t^{1/3}$ was derived. The same scaling law was obtained by Tang & Tang (1994) using similar assumptions. However, for a moving corner film, the capillary pressure should be balanced with both the hydrostatic head and the viscous friction. Ponomarenko et al. (2011) used a capillary bundle model to characterize the corner film and compared the imbibition dynamics in each sub-capillary considering gravity. The imbibition speed in each sub-capillary was calculated and the leading sub-capillary with the radius of r_L which has the maximum imbibition speed was found approaching the vertex of the corner as $r_L \propto t^{-1/3}$. Based on this assumption a universal scaling law of $h \propto t^{1/3}$ was derived for the corner film. However, the derivation of equation (4.2) in their work shows some limiting assumptions, making the results less accurate, which will be improved in this paper.

Among these mathematical models, the capillary bundle model is the simplest and easiest one. However, the main limitation of this capillary bundle model to describe the imbibition with corner films is that the interactions between different sub-capillaries are not considered. As a result, the imbibition velocity in the main meniscus can happen to be higher than that of the arc meniscus (Ponomarenko et al., 2011), which is in conflict with other numerical simulation results (Gurumurthy et al., 2018). We will show in this paper that the arc meniscus always imbibes faster than the main meniscus. To overcome this limitation, we propose to use an interacting capillary bundle (ICB) model to describe the imbibition dynamics with corner films. The ICB model was firstly proposed by Dong et al. (Dong et al., 2005; Dong & Zhou, 1998) in which interactions between connecting capillaries are considered. This model was mainly used to describe the imbibition process in porous media at continuum scale (Li et al., 2017; Wang et al., 2012) rather than in a single pore. In this work, a modified ICB model is developed to describe the imbibition dynamics in a single square tube.

Numerical methods are very helpful tools to understand the underlying mechanisms of multiphase flow in porous media and to validate analytical models (Golparvar et al., 2018; Zhao et al., 2019). The different numerical methods to simulate multiphase fluid flow mainly include computational fluid dynamic (CFD) which couples the Navier–Stokes equations with interface-capturing methods (Zhang et al., n.d.; Zhu, Chen, et al., 2019; Zhu, Kou, et al., 2019), the lattice

Boltzmann method (LBM) (Chen et al., 2014; Huang et al., 2015; Liu et al., 2016; Qin et al., 2018, 2019, 2020; Sukop, 2006), the dissipative particle dynamics method (Groot & Warren, 1997) and the smoothed particle hydrodynamics method (Yang et al., 2020), etc. Raiskinmäki et al. (2002) used LBM to simulate the imbibition dynamics in a circular tube and the simulation results matched well with the theoretical solutions both with and without considering gravitational forces. Son et al. (2016) used a pseudopotential multiphase LB model to study the influence of contact angle on arc menisci in polygonal tubes and validated the simulation results with the Mayer and Stoewe-Princen (MS-P) theory. Gurumurthy et al. (2018) used the CFD with the solver OpenFOAM to simulate liquid imbibition dynamics in a square tube with corner films and analyzed the influences of different parameters on the imbibition dynamics. The shapes of the corner films were analyzed in detail. In this work, we use LBM to validate the modified ICB model and to analyze the underlying mechanisms during imbibition process. More specifically, a color-gradient lattice Boltzmann model is used, which has proven to be an accurate method to simulate multiphase flow in porous media (Chen et al., 2019; Zhao et al., 2018, 2020).

The corner film is also important during drying of a porous material, which can significantly improve the drying rate (Lal et al., 2019; Laurindo & Prat, 1998). Through analyzing the drying process in a square tube with both microscale experiment and numerical simulation, Chauvet et al. (2009) observed three drying periods including the constant rate period, falling rate period and receding front period. The corner film was found to play an important role in the transition between different periods. Wu et al. (2020) conducted microfluidic experiments of liquid drying from a strong liquid wetting pore network. It was found that the main meniscus invades faster into the pore network, leaving liquid films residual in the corners. The continuous wetting corner films connected to the bulk liquid fluid significantly increased the drying rate. In addition, a pore network model considering corner film flow was developed which matched well with the experimental results. In the current work, we mainly focus on the spontaneous imbibition in an angular tube without phase change phenomenon. However, the modified ICB model developed in this work could be potentially extended in future to account for liquid drying with corner films, which has a broad range of applications. For example, in passive desalination of seawater, capillary action plays an important role in the photothermal materials (Arunkumar et al., 2020), which could supply water to the evaporative region to sustain the incoming heat flux by incident light. The porous wicking

materials should be well designed to ensure strong water transport and mitigates salt crystallization or migration.

This paper is arranged as follows. In section 2, we propose a modified ICB model to describe spontaneous imbibition in a square tube with corner films, where the local capillary pressure and conductance are derived based on the specific shape of each sub-capillary. In section 3, the color-gradient lattice Boltzmann method is briefly introduced and validated, and the simulation setups are also described. In section 4, both the modified ICB model and LBM are used to simulate the spontaneous imbibition in a square tube with different fluid properties. The accuracy of the modified ICB model is verified by comparisons between the ICB and LBM simulation results. In this section, the influences of different parameters on the imbibition process are also investigated. In section 5, we further discuss the scaling law of imbibition dynamics for both the main and arc menisci during the imbibition process. The conclusions are summarized in section 6.

2 Theoretical model: interacting capillary bundle model

2.1 General model description

In this work, a modified ICB model is used to describe the imbibition dynamics in a square tube considering corner films. **Figure 2** shows the schematic of an interacting capillary bundle model for the liquid-gas system which consists of n capillaries. p_{ci} is the capillary pressure in the i-th capillary, which is the driving force for spontaneous imbibition. $h_{i,t}$ is the imbibition length (height) in the i-th capillary at time t. As the density and dynamic viscosity of the gas phase are much smaller than those of the liquid phase, we neglect the hydrostatic pressure drop and viscous dissipation in the gas phase to make the model simpler, which results in a constant pressure in gas phase. In the ICB model, fluid can flow laterally between two connecting capillaries with no flow resistance. Therefore, the pressure drop in the lateral direction is neglected, which means the liquid phases have the same pressure in different capillaries at the same position h. Accordingly, the pressure distribution along the imbibition height is shown as the solid line.

At a given time *t*, for a certain range of imbibition length $h_{i-1,t}<h<h_{i,t}$ ($i>1$), the driving pressure difference Δp_i is the capillary pressure difference between the (i-1)th and i-th capillaries:

$$\Delta p_i = p_{ci} - p_{ci-1} \tag{4}$$

We focus on the viscous regime in this work, therefore the inertial force is neglected. As a result, the resistance forces consist of two parts: viscous dissipation and gravitational force. For the i-th capillary, the relationship between volume flux (q) and viscous pressure drop over a certain length Δh_i can be calculated by:

$$q_i = g_i \frac{\Delta p_{vis,i}}{\Delta h_i} \tag{5}$$

where g_i is the conductance of the i-th capillary dependent on the shape of the capillary. g_i can be calculated with the following expression which is widely used in pore network modeling (Zhao et al., 2020):

$$g_i = c_i \frac{A_i^2 G_i}{\mu}, \tag{6}$$

where A is the cross section area of the i-th capillary. G is the shape factor which is defined as A/P^2, where P is the perimeter of the cross section. μ is the dynamic viscosity of the liquid phase. c_i is the modification coefficient which depends on the shape of the cross section. As shown in **Figure 2**, for $h_{i-1,t}<h<h_{i,t}$, the wetting phase can imbibe into the capillaries in which the capillary pressure is larger than p_{ci-1}. Therefore, the total liquid volume flux in this range can be calculated by:

$$\sum_{k=i}^{n} q_{k,t} = \sum_{k=i}^{n} \left(g_k \frac{\Delta p_{vis,i}}{\Delta h_i} \right) \tag{7}$$

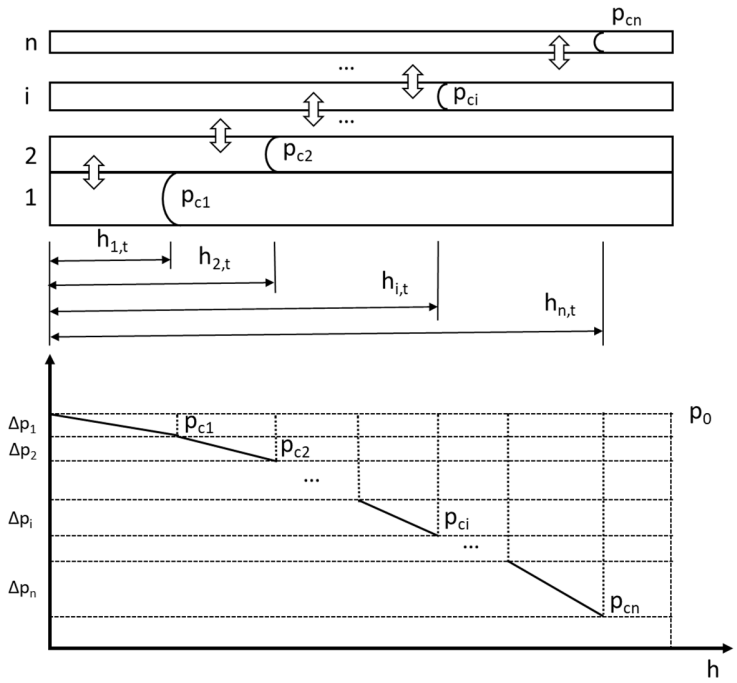

Figure 2. Schematic of the interacting capillary bundle model for liquid-gas system. Liquid imbibition from left side of the capillaries.

Taking $\Delta h_i = h_{i,t} - h_{i,t-1}$, the viscous pressure drop from $h_{i-1,t}$ to $h_{i,t}$ is:

$$\Delta p_{vis,i,t} = \frac{\left(h_{i,t} - h_{i-1,t}\right)}{\sum_{k=i}^{n} g_k} \sum_{k=i}^{n} q_{k,t} \tag{8}$$

The pressure drop caused by gravity is:

$$\Delta p_{g,i,t} = \rho g \left(h_{i,t} - h_{i-1,t}\right) \tag{9}$$

Finally, the driving force is balanced by the resistance force in terms of pressure difference:

$$\frac{\left(h_{i,t} - h_{i-1,t}\right)}{\sum_{k=i}^{n} g_k} \sum_{k=i}^{n} q_{k,t} + \rho g \left(h_{i,t} - h_{i-1,t}\right) = p_{ci} - p_{ci-1}, \quad i = 2,3,...,n \tag{10}$$

For the first part from 0 to $h_{1,t}$, we have:

$$\frac{h_{1,t}}{\sum_{k=1}^{n} g_k} \sum_{k=1}^{n} q_{k,t} + \rho g h_{1,t} = p_{c1} \tag{11}$$

The volume flux in the *k*-th capillary can be approximated by the following expression (Dong et al., 2005):

$$q_{k,t} = A_k \left(\frac{dh_{k,t}}{dt} \right) \approx A_k \frac{h_{k,t} - h_{k,t-\Delta t}}{\Delta t} \tag{12}$$

Combining equations (10) - (12), the following equations are obtained and can be solved with Newton's iteration method (Dong et al., 2005).

$$\begin{cases} \dfrac{\left(h_{i,t} - h_{i-1,t}\right)}{\sum_{k=i}^{n} g_k} \sum_{k=i}^{n} A_k \dfrac{h_{k,t} - h_{k,t-\Delta t}}{\Delta t} + \rho g \left(h_{i,t} - h_{i-1,t}\right) = p_{ci} - p_{ci-1}, \quad i > 1 \\ \dfrac{h_{1,t}}{\sum_{k=1}^{n} g_k} \sum_{k=1}^{n} A_k \dfrac{h_{k,t} - h_{k,t-\Delta t}}{\Delta t} + \rho g h_{1,t} = p_{c1}, \quad i = 1 \end{cases} \tag{13}$$

2.2 Modified interacting capillary bundle model for the square tube

2.2.1 Decomposition of the square tube

In the modified ICB model, the square tube is decomposed into several interacting sub-capillaries to describe the imbibition dynamics of a wetting liquid. According to equation (13), the imbibition process is determined by three parameters: the conductance g_k, the cross section area A_k and the capillary pressure p_c in each sub-capillary. To keep as much information as possible, the square tube is decomposed into several sub-capillaries without shape simplification. **Figure 3** (a) shows one example of the decomposition result of a square tube. Due to the symmetry of the square tube, the imbibition process in all the four corners is the same. Therefore, only one quarter of the square tube is shown. The decomposition follows the following three steps.

First, the critical radius (R_c) of a square tube is calculated by the following equation at a given contact angle ($\theta < \pi/4$) (Dong & Chatzis, 1995):

$$R_c = \frac{W}{2}\left(\frac{\cos\theta - \sqrt{(\pi/4-\theta)+\sin\theta\cos\theta}}{(\theta-\pi/4)+\cos^2\theta-\sin\theta\cos\theta}\right), \tag{14}$$

where W is the side length of the square tube. The corresponding capillary pressure $p_c = \gamma/R_c$ is the entry capillary pressure of this tube. The arc line with radius of R_c is selected as the boundary of the first sub-capillary, shown as red line in **Figure 3** (a). The first sub-capillary corresponds to the main meniscus in the square tube.

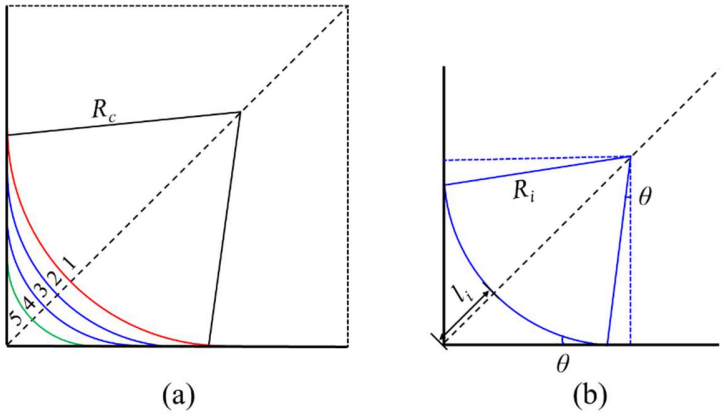

Figure 3. Decomposition of the square tube into interacting capillary bundles of different shapes. Only one quarter of the square tube is shown.

As shown in **Figure 3** (b), the length from the arc line to the vertex of the corner (l_i) can be calculated as:

$$l_i = \left(\sqrt{2}\cos\theta - 1\right)R_i \tag{15}$$

By setting R_i=R_c, we obtain the maximum length l_{max} according to above equation.

Second, we set a minimum l_i (l_{min}) for the interacting capillary bundle model. The corresponding radius R_{min} can be also calculated by equation (15). The arc line with radius of R_{min}, shown with a green line in **Figure 3** (a), is the boundary of the last sub-capillary.

Finally, we decrease l_i from l_{max} to l_{min} with a constant step of $\Delta l = (l_{max} - l_{min})/(N_c - 2)$, where N_c is the total number of interacting sub-capillaries, which is 5 in **Figure 3** (a). The corresponding radii R_i are calculated based on l_i and equation (15). The arc lines with radii of R_i are shown as blue lines in **Figure 3** (a), which are the boundaries for the different sub-capillaries.

The first sub-capillary corresponds to the main meniscus of the tube and all the other sub-capillaries correspond to the arc meniscus in this corner.

According to this decomposition process, only $l_{\max}$ is determined for a certain square tube with a given contact angle. The values for $l_{\min}$ and N_c are self-defined. In section 4.1 we analyze the influence of both parameters on the imbibition process.

2.2.2 Cross-section area and local capillary pressure of each sub-capillary

Based on geometric analysis of **Figure 3**, the cross-section area of each sub-capillary can be calculated by:

$$\begin{cases} A_1 = W^2/4 - R_c^2\left[\cos^2\theta - \sin\theta\cos\theta - (\pi/4-\theta)\right], & i=1 \\ A_i = \left(R_{i-1}^2 - R_i^2\right)\left[\cos^2\theta - \sin\theta\cos\theta - (\pi/4-\theta)\right], & 1<i<N_c \\ A_{N_c} = R_{N_c}^2\left[\cos^2\theta - \sin\theta\cos\theta - (\pi/4-\theta)\right], & i=N_c \end{cases} \tag{16}$$

When the wetting phase contact angle is smaller than $\pi/4$, the wetting liquid meniscus in the corner develops faster than the main meniscus, forming a long arc meniscus in the corner along the axis of the tube. Therefore, the curvature of the arc meniscus in the plane perpendicular to the axis of the tube is much larger than that in the plane along the axis of the tube. Neglecting the curvature in the direction parallel to the axis of the tube, the local capillary pressure can be calculated by $p_c = \gamma/R_i$ for the arc meniscus shown in **Figure 3** (b). For the sub-capillaries shown in **Figure 3** (a), we calculate the local capillary pressures by:

$$\begin{cases} p_{c1} = \gamma/R_c, & i=1 \\ p_{ci} = 2\gamma/\left(R_{i-1}+R_i\right), & 1<i<N_c \\ p_{cN_c} = \gamma/R_{N_c}, & i=N_c \end{cases} \tag{17}$$

2.2.3 Flow conductance of each sub-capillary

For the regular capillary, the conductance can be calculated by analytical or empirical expressions (Zhao, et al., 2020). However, the decomposed sub-capillaries in this work are quite irregular and the corresponding conductances cannot be calculated analytically. Therefore, the flow conductance of each sub-capillary is calculated based on single-phase lattice Boltzmann simulation (Zhao, et al., 2020). **Figure 4** shows the cross section of a square tube with a side

length of 400 lattices. This cross section is extended in *z* direction with 3 lattices. Then a multi-relaxation-time single-phase lattice Boltzmann model is used to simulate external-force-driven single-phase flow in this tube. The fluid density is set as 1.0 and the kinetic viscosity is set as 0.5. A small external acceleration a_z=5.0×10^{-6} is imposed in *z* direction and periodic boundary conditions are considered. When the relative volume flow rate change in 100 consecutive simulation steps becomes less than 10^{-6} we assume the simulation has reached the steady state.

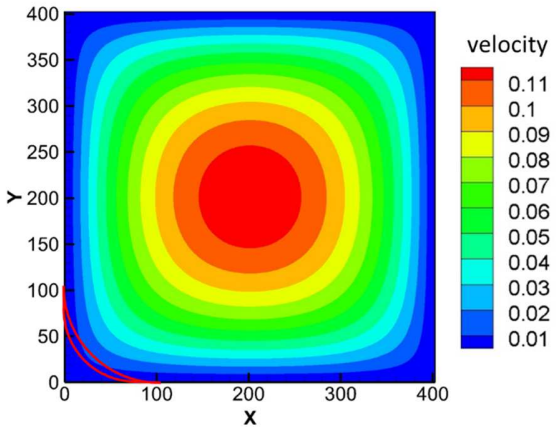

Figure 4. Velocity distribution in a square tube simulated by single-phase lattice Boltzmann method. The velocity is in lattice units.

Figure 4 shows the steady sate velocity distribution in this tube in lattice unit. To calculate the conductance of a sub-capillary, the cross section of this sub-capillary is firstly mapped onto the whole square tube. The region outlined by red lines in **Figure 4** shows one typical cross section of a sub-capillary *i* (1<*i*<N_c). Then the volume flux across this sub-capillary (q_i) is calculated by integrating the velocity distribution within the marked region. The conductance of this sub-capillary can be calculated by (Zhao et al., 2020)

$$g_i = \frac{q_i}{\rho a_z}\frac{\mu_{LBM}}{\mu}, \tag{18}$$

where μ_{LBM} is the dynamic viscosity used in LBM simulation and μ is the dynamic viscosity used in the modified ICB model. It should be mentioned that, as lattice units are used in this simulation, the obtained conductance can be rescaled and applied in the square tube with different dimensions when appropriate scaling is used for length, time and mass (Zhao et al., 2020).

3 Numerical model

3.1 Color-gradient lattice Boltzmann method

In this work, a multi-relaxation-time color-gradient lattice Boltzmann model is used to simulate and analyze the spontaneous imbibition process in a square tube. The results are also used to validate the accuracy of the modified ICB model. The color-gradient LBM is a multicomponent multiphase lattice Boltzmann model which uses two density distribution functions to represent the immiscible two fluids. This model has been widely used to simulate two-phase flow in porous media (Huang et al., 2014; Liu et al., 2014, 2015; Zhao et al., 2018). The details of the model can be found in the references (Liu et al., 2012; Xu et al., 2017; Zhao et al., 2018; Zhao et al., 2020).

To realize the no-slip velocity on solid surfaces, the halfway bounce-back boundary condition is used. To achieve a specific contact angle, a recently developed wetting boundary condition is used in this work, which is based on the geometry of the solid surface and yields a more accurate contact angle and much smaller spurious velocity (Akai et al., 2018; Chen et al., 2019; Leclaire et al., 2017; Xu et al., 2017).

3.2 Model validation

3.2.1 Contact angle test

The contact angle is a decisive parameter in determining the imbibition process in an angular tube. The corner film can be developed only when $\theta < \pi/2 - \alpha/2$. Therefore, we evaluate the accuracy of the color-gradient LBM in achieving a specific contact angle. As demonstrated previously (Chen et al., 2019), the accuracy of simulated contact angle is related to the viscosity ratio. In this work, we focus on the liquid-gas system with dynamic viscosity ratio (M) between liquid and gas set at M=73.5. At initial condition we put a non-wetting gas bubble in the liquid on a flat surface. We let the bubble evolve and once steady state is reached, the contact angle is measured. Different liquid contact angles, ranging from 10° to 90°, are evaluated in this work and the relationship between the prescribed contact angle and simulated contact angle is plotted in **Figure 5**. As can be seen from this figure, the relationship is very good in the 60-90° range. Below this range, the simulated contact angle deviates slightly from the

prescribed one, but the deviation remains acceptable for our investigation. In the following description, when we mention the contact angle, we refer to the simulated one, not the prescribed one.

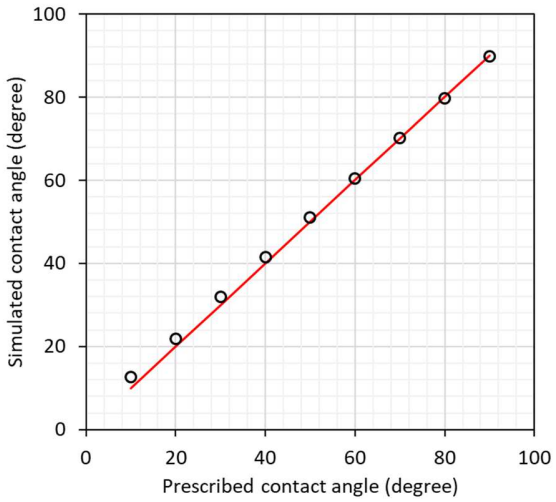

Figure 5. Comparison between prescribed and simulated contact angles.

3.2.2 Imbibition in a circular tube

The imbibition dynamics in a circular tube is simulated with LBM and the simulation results are compared with theoretical solutions to verify the accuracy of LBM. In this validation, the radius of the circular tube is 500 μm; the densities of the liquid and gas phases are 750 kg/m^3 and 1.18 kg/m^3, respectively; the dynamic viscosities of the liquid and gas phases are 6.8 mPa·s and 0.0925 mPa·s, respectively, and the surface tension between the two fluids is 0.024 N/m. The liquid fluid is the wetting phase and three different wetting phase contact angles are considered, 60.5°, 21.9° and 12.6°, respectively. The physical units are transferred into lattice units using dimensionless numbers including Capillary number (*Ca*) which represents the ratio between viscous to surface tension forces, Ohnesorge number (*Oh*) which means the ratio between viscous to inertial and surface tension forces, and Bond number (*Bo*) which indicates the ratio between gravitational to surface tension forces. It should be mentioned that the same densities are used in the LBM simulation for liquid and gas phases to keep the model stable, which is $\rho_l = \rho_g = 1.0$. The influence of gravity is introduced with different gravitational forces. If gravity is considered, the gravitational accelerations for both fluids are $g_l = 2.205\times10^{-6}$ and

$g_g = 3.4692\times10^{-9}$, respectively, which are obtained based on the above mentioned dimensionless numbers. As demonstrated in the following validation, this treatment has negligible influence on the accuracy of the imbibition dynamics in the tube. As a result, in lattice units, the viscosities of the liquid and gas phases are $\mu_l = 0.136$ and $\mu_g = 0.00185$, respectively and the surface tension is 0.072.

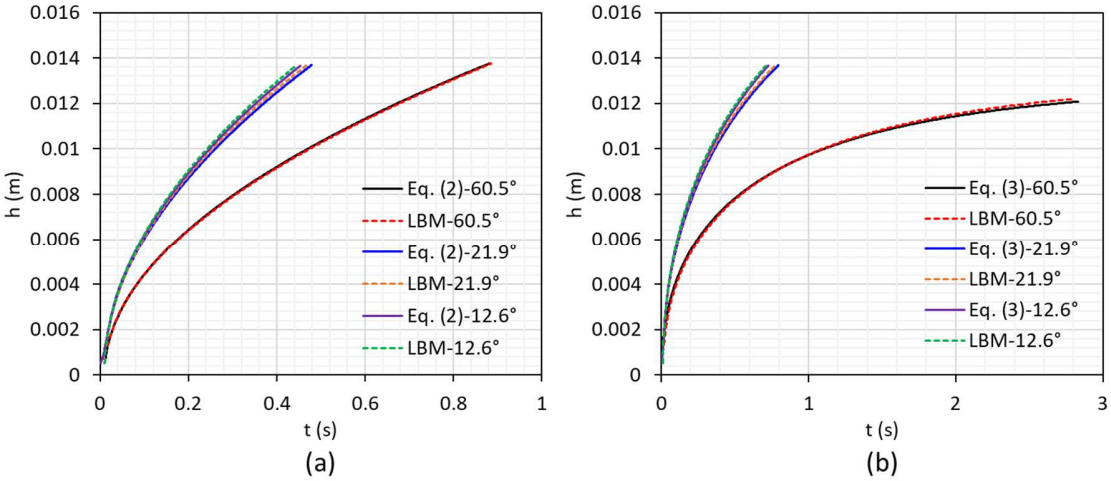

Figure 6. Comparison of the imbibition dynamics in a circular tube obtained by Washburn equation and LBM (a) without gravity; (b) with gravity.

A circular tube with inscribed radius of 25 lattices and length of 1400 lattices in *z* direction is constructed. At initial condition, the non-wetting gas phase fills most of the tube and a small amount of wetting liquid phase is located at the bottom of the tube. The pressure boundary conditions are used at the bottom and top boundaries with the same pressure value to simulate the spontaneous imbibition process. The relationships of imbibition length versus time are plotted in **Figure 6** for the cases with (a) and without gravity (b). The theoretical solutions are calculated based on equations (2) and (3) shown in the introduction. It should be mentioned that the two-phase interface is initialized as a flat interface at the beginning of the simulation and it takes some time for the interface to reach an equilibrium shape. To eliminate the influence of this early period, the start time of the theoretical model is adjusted a little compared to the LBM curve. As can be seen in **Figure 6**, the LBM simulation results match well with the theoretical solutions for different wetting phase contact angles, both with and without gravitational force, demonstrating the accuracy of LBM to simulate the imbibition dynamics in a tube. In addition,

the strategy of using the same density but different gravitational forces is found to be appropriate to consider the influence of gravity.

3.3 Simulation setup

This work focuses on the spontaneous imbibition in the square tube considering corner films. Due to the symmetry of the square tube, we only simulate the imbibition dynamics in one quarter of the tube to save computational resources. The schematic of the simulation domain is shown in **Figure 7**. The black box shows the whole square tube, while the blue box shows one quarter of the square tube, as considered in our simulation. The initial condition and pressure boundary conditions on the top and bottom boundaries are the same as those introduced in section 3.2.2. Two sides, the back and left boundaries, are solid walls and wetting boundary conditions combined with halfway bounce-back boundary conditions are applied. For the two other sides of the blue domain, the symmetry boundary conditions are adopted on the front and right boundaries.

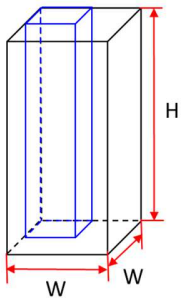

Figure 7. Schematic of the simulation domain of square tube.

The accuracy of LBM simulation results increases with grid number. After sensitivity analysis, we select W=100 lattices. Five cases listed in **Table 1** are considered to analyze the imbibition dynamics in the square tube with corner films in order to investigate the influences of different parameters on the imbibition dynamics. Case1 is the base case. In Case2 the dynamic viscosities of both fluid and gas are changed. In Case3 the surface tension is doubled and the height of the tube is increased. In Case4, the contact angle is decreased, while in Case5 the height is increased considering no gravity.

Table 1. Different cases for spontaneous imbibition analysis.

	W (μm)	H (mm)	ρ_l (kg/m^3)	ρ_g (kg/m^3)	μ_l (mPa·s)	μ_g (mPa·s)	γ (N/m)	g (m/s^2)	θ (°)
Case1	700	11.2	750	1.18	6.8	0.0925	0.012	9.8	21.9
Case2	700	11.2	750	1.18	13.6	0.185	0.012	9.8	21.9
Case3	700	17.64	750	1.18	6.8	0.0925	0.024	9.8	21.9
Case4	700	11.2	750	1.18	6.8	0.0925	0.012	9.8	12.6
Case5	700	17.64	750	1.18	6.8	0.0925	0.012	0	21.9

4 Results and analysis

In this work, both the modified ICB model and LBM are used to predict the imbibition dynamics in a square tube with corner films. The LBM simulation results are used to verify the accuracy of the modified ICB model. In addition, the influences of different parameters on the imbibition dynamics are investigated and the underlying mechanisms are analyzed.

4.1 Sensitivity analysis of the modified interacting capillary bundle model

As stated in section 2.2.1, the length $l_{\min}$ and number of interacting sub-capillaries N_c are self-defined parameters in the modified ICB model. To analyze the influences of both parameters on the results of the modified ICB model and to select optimal values, a sensitivity analysis of these two parameters is performed. The fluid properties in Case1 are used in this analysis. First, $l_{\min}$ is set as $l_{\min}=0.1l_{\max}$, where $l_{\max}$ is obtained from equation (15). Different values of N_c ranging from 3 to 9 are used to predict the imbibition dynamics and the results are shown in **Figure 8**. **Figure 8** (a) shows the relationship between imbibed wetting liquid volume versus time and **Figure 8** (b) shows the imbibition heights in different sub-capillaries, where "center" refers to the imbibition height in the first sub-capillary, which corresponds to the main meniscus in the center, while "corner" represents the last sub-capillary, which corresponds to the height of the corner film. As shown in **Figure 8** (a), the imbibed wetting liquid volume is not very sensitive to N_c and the curves for different values of N_c almost coincide with each other. The main reason is that the total imbibed wetting phase volume mainly depends on the imbibition length in the first sub-capillary representing the main meniscus, which is insensitive to N_c, as shown in **Figure 8** (b). However, N_c has some influence on the imbibition dynamics in the corners. As shown in **Figure 8** (b), when N_c is too small (N_c=3), the imbibition height in the last sub-capillary is underestimated. When N_c is larger than 5, the imbibition dynamics obtained with

different values of N_c almost coincide with each other. In conclusion, the prediction results of the modified ICB model is insensitive to N_c when $N_c \geq 5$. In the following analysis, we set N_c=7.

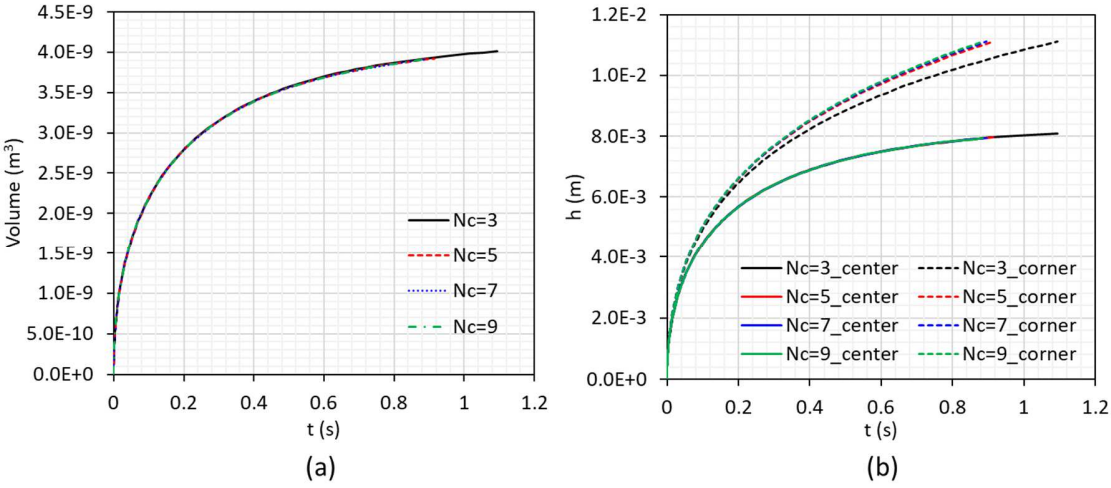

Figure 8. Influence of number of sub-capillaries N_c on the prediction results of the modified interacting capillary bundle model (a) relationship between wetting phase volume and time; (b) imbibition height versus time at different positions of the square tube.

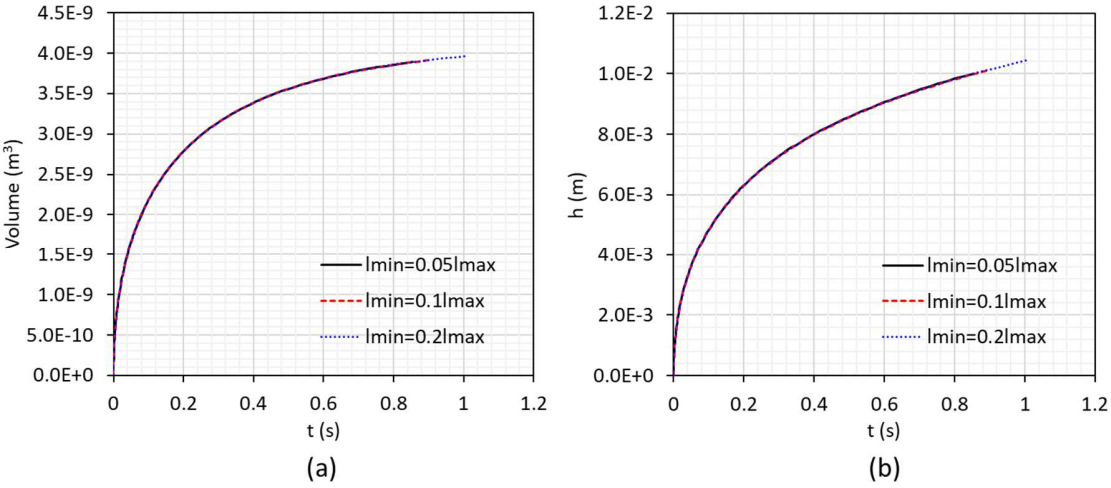

Figure 9. Influence of length l_{min} on the prediction results of the modified interacting capillary bundle model. (a) relationship between wetting phase volume and time; (b) imbibition height versus time at a certain position of the square tube.

Next, the influence of the length l_{min} of the last sub-capillary is analyzed by setting different values of l_{min}, namely $0.05l_{max}$, $0.1l_{max}$ and $0.2l_{max}$ while N_c is fixed to 7. **Figure 9** shows the imbibition dynamics predicted by the modified ICB model with different l_{min}. **Figure 9** (a) shows the imbibition volume versus time. As a smaller l_{min} results in a higher imbibition

height of the last sub-capillary, in order to compare the prediction results for different l_{min}, we plot the imbibition height versus time at the same position of the corner with l=22.5μm in **Figure 9** (b), where l is the distance to the vertex of the corner in the diagonal of the tube, as shown in **Figure 3** (b). It should be mentioned that l=22.5μm corresponds to the center of the fifth sub-capillary when l_{min}=0.1l_{max}. Therefore, h shown in **Figure 9** (b) is the imbibition height of the fifth sub-capillary when l_{min}=0.1l_{max}. While for l_{min}=0.05l_{max} (l_{min}=0.2l_{max}), the position of l=22.5μm locates between the fourth and fifth (fifth and sixth) sub-capillaries and h in **Figure 9** (b) is obtained by linear interpolation of the imbibition heights of these two adjacent sub-capillaries. According to the prediction results, l_{min} has no influence on the imbibition volume and imbibition height at the same position of the corner (l=22.5μm) with N_c=7 when l_{min}<0.2 l_{max}. Therefore, in the following analysis we set l_{min}=0.1l_{max} and N_c=7. It should be mentioned that a smaller l_{min} also results in a higher equilibrium height of the last sub-capillary due to the larger capillary pressure. We have also tested the influences of both parameters for other fluid properties and contact angles and came to the same conclusion.

4.2 Comparison of the interface profiles at different times

After selecting the values of l_{min} and N_c in the modified ICB model, both LBM and the modified ICB models are used to predict the liquid imbibition dynamics in a square tube for Case1. For the LBM simulation, at initial condition, the tube is filled mostly with gas phase and a small amount of liquid phase is located at the bottom of the tube, as shown in **Figure 10** at t=0. As time goes, the liquid phase invades into the tube. At the early stage of imbibition, the arc meniscus in the corner is slightly higher than the main meniscus in the center, as shown in **Figure 10** at t=40000 and 80000. Later on, after t>160000, the arc meniscus in the corner develops faster than the main meniscus and the arc meniscus becomes more and more prominent. The origin of this mode of evolution is discussed in section 4.3. To compare the results of the modified ICB model with the LBM simulation results, the interface profile seen in a plane set diagonally across the tube is plotted at different times, as shown in **Figure 11**. The solid lines show the interface profiles obtained by LBM simulation, which correspond to the five in-progress configurations shown in **Figure 10**. The modified ICB model imbibition heights in seven sub-capillaries are plotted for the same five imbibition times. As shown in **Figure 11**, the arc meniscus becomes lengthening with time. In general, the prediction results of the modified

ICB model match well with the LBM simulation results, demonstrating the possibility of using the modified ICB model to describe the imbibition dynamics in a square tube with corner films. We observe that the imbibition heights of the main meniscus predicted by the modified ICB model are always slightly higher than the LBM simulation results. This may be caused by several possible reasons as discussed next. The modified ICB model consists of several 1D sub-capillaries. For each sub-capillary, there is only one imbibition height. In the LBM simulation, the main meniscus is a curved interface, as shown in **Figure 10**. By averaging the curved interface of the main meniscus to a flat surface, the obtained imbibition height would be slightly higher than the imbibition height at the center of the tube. In addition, the flow resistance of gas phase is neglected in the modified ICB model, which may make the imbibition process faster. Finally, the ICB model is based on simplifications, which may also cause some difference with the more accurate LBM simulation results.

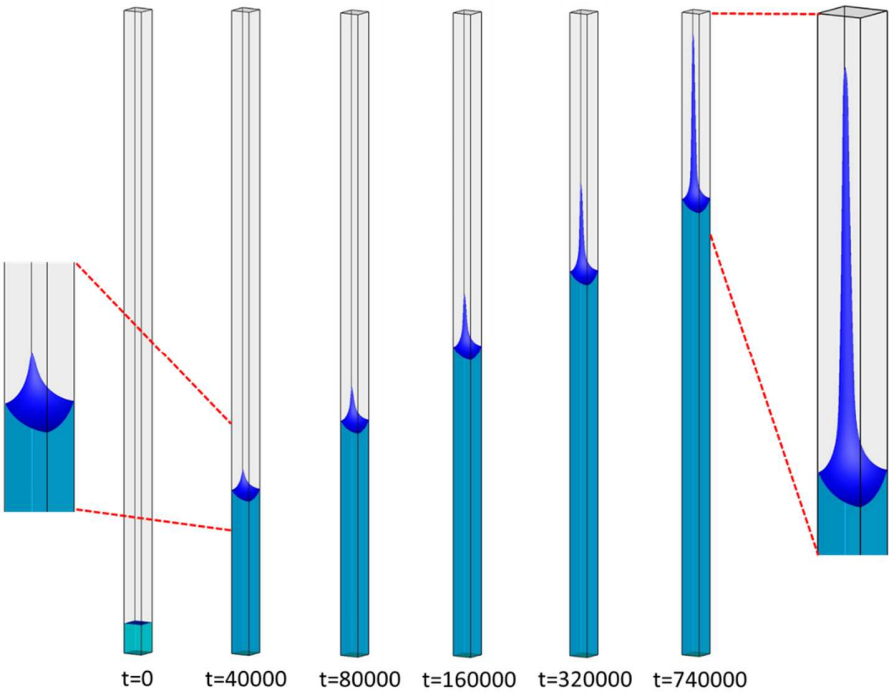

Figure 10. Wetting liquid distributions obtained by LBM at different simulation steps.

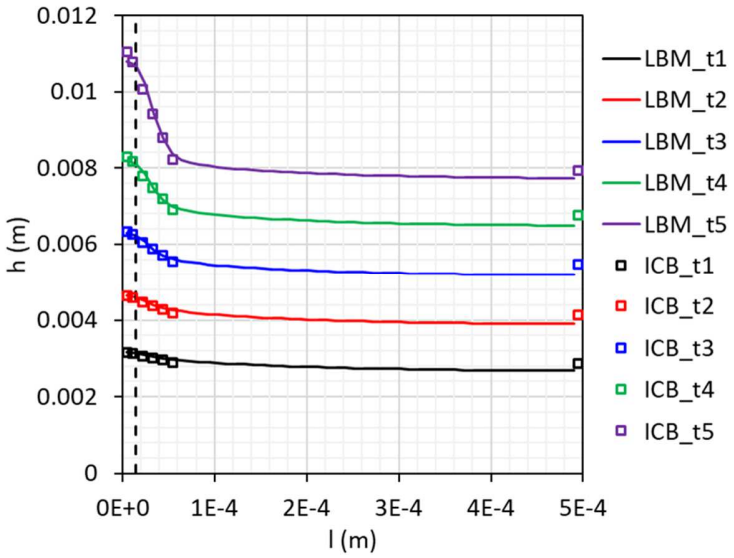

Figure 11. Comparison of interface profiles at different imbibition times.

4.3 Imbibition dynamics in square tube

The imbibition dynamics for Case1 obtained by LBM simulation and the modified ICB model are compared, as shown in **Figure 12**. **Figure 12** (a) shows the imbibed wetting liquid volume versus time and **Figure 12** (b) shows the imbibition lengths of both main meniscus and arc meniscus versus time. The imbibition length of main meniscus corresponds to the center of the tube in LBM simulation and the first sub-capillary in the modified ICB model, while the imbibition length of arc meniscus shows the imbibition length at l=14.8μm for both LBM simulation and the modified ICB model, marked as dashed solid line shown in **Figure 11**. Similar to the validation in section 3.2.2, the start time of the modified ICB model is shifted a little from 0 to eliminate the influence of the early period when the interface evolves from a flat surface to an equilibrium shape. All the curves stop at the same imbibition height of arc meniscus. As can be seen, for both the imbibed wetting liquid volume and imbibition length, the prediction results of the modified ICB model match well with the LBM simulation results.

In addition, from **Figure 12** (b) we observe that the imbibition length of arc meniscus is always higher than that of the main meniscus, meaning that the arc meniscus is always advancing faster than the main meniscus does. We remark the non-interacting capillary bundle model of Ponomarenko et al. (2011) did not uncover this phenomenon, which can be well captured by the modified ICB model. In **Figure 12** (b), the predictions of the original interacting capillary bundle

(OICB) model, as per Dong et al. (2005), which only consists of circular sub-capillaries, are also plotted for comparison, shown as dash-dot lines. As can be seen, the OICB model can well describe the imbibition dynamics of the main meniscus, because the driving and resistance forces of the main meniscus in a square tube are similar to those in a circular tube. However, for the sub-capillaries in the corners, the OICB model fails to accurately capture the relationship between driving and resistance forces, resulting in a poor prediction of the imbibition dynamics of the arc meniscus. As the modified ICB model keeps the real geometry of the filled corners, it describes well the imbibition dynamics of both main and arc menisci.

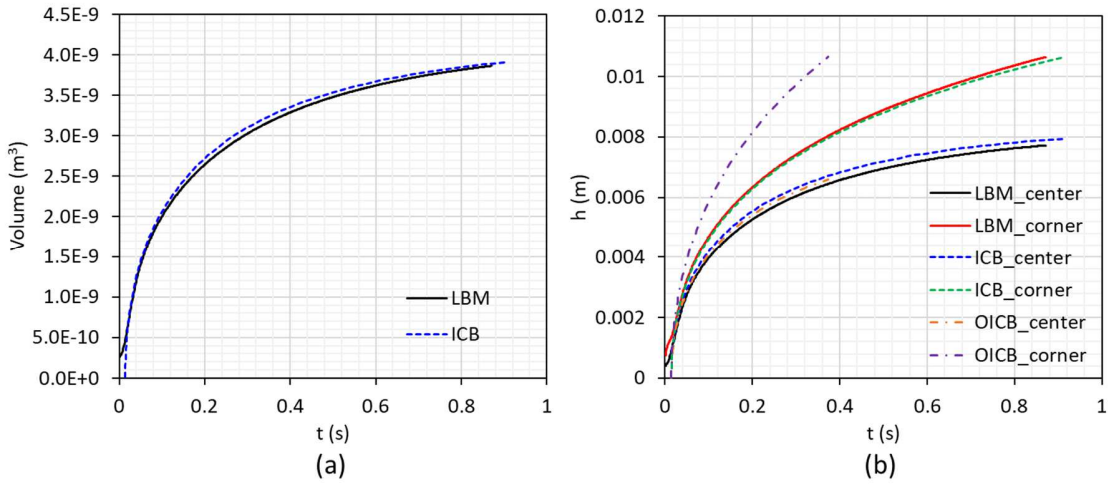

Figure 12. Imbibition dynamics in a square tube. (a) relationship between wetting fluid volume and time; (b) imbibition length of main and arc menisci obtained by LBM and two different ICB models, where center refers to the main meniscus in the center of the tube and corner means the arc meniscus in the corner. ICB represents the modified interacting capillary bundle model developed in this work; OICB refers to the original interacting bundle model which consists of circular sub-capillaries.

Using the modified ICB model, we further analyze the imbibition dynamics of main and arc menisci in a square tube. **Figure 13** (a) shows the imbibition lengths versus time for each sub-capillary. As can be seen, at early times, the imbibition lengths in the different sub-capillaries are similar. As time goes on, the water in the corners moves ahead of the main meniscus, identified as the 7th sub-capillary. This is mainly due to gravity as will be explained below. For spontaneous imbibition in a square tube, the driving force is the capillary force and the resistance force includes viscous and gravitational forces when gravity is considered. For a certain sub-capillary in the modified ICB model, the pressure difference (Δp_c) caused by

capillary force is a constant, while the pressure difference (Δp_g) caused by gravitational force increases with the imbibition height. **Figure 13** (b) shows the proportion of Δp_g to Δp_c in the seven sub-capillaries versus time. With the imbibition process going on, $\Delta p_g / \Delta p_c$ increases rapidly in the first sub-capillary, i.e. the main meniscus. The pressure difference driving the imbibition process ($\Delta p_c - \Delta p_g$) decreases accordingly, leading to a slower imbibition velocity of the main meniscus. In contrast, $\Delta p_g / \Delta p_c$ increases much less for the other sub-capillaries forming the corner film, with the smallest influence of gravity in the last sub-capillary showing the highest capillary pressure. These different trends in the main meniscus and the other sub-capillaries mainly arise from the difference in the acting driving and resistance forces. For the main meniscus, Δp_c is the capillary pressure of main meniscus and Δp_g the pressure difference from the bottom of the tube to the main meniscus caused by gravitational force. Δp_g increases linearly with the imbibition height of main meniscus. However, for the other sub-capillaries in the corners, the driving force is the capillary pressure difference between connecting sub-capillaries and the resistance gravitational force is caused by the different imbibition heights in the connecting sub-capillaries. For example, for the second sub-capillary which connects to the first sub-capillary (main meniscus), Δp_c represents the capillary pressure difference of the second sub-capillary and main meniscus, and Δp_g is the pressure difference between the imbibition heights in these two sub-capillaries cased by gravitational force. Δp_g increases linearly with the imbibition height difference between these two sub-capillaries. As shown in **Figure 13** (a), the main meniscus quickly invades into the tube while the imbibition height difference between connecting sub-capillaries grows slowly. As a result, $\Delta p_g / \Delta p_c$ shows different trends for the main meniscus and sub-capillaries in the corners.

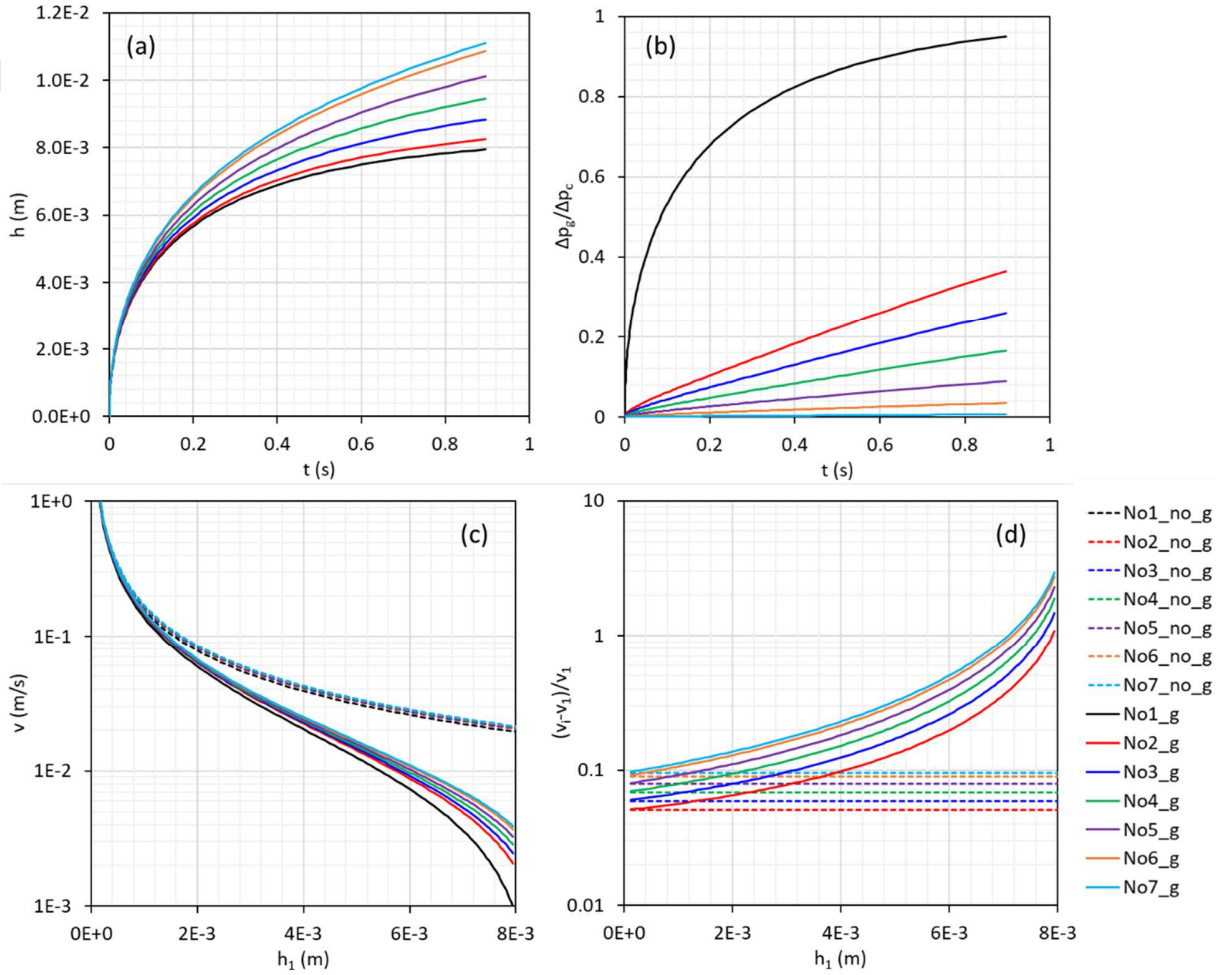

Figure 13. Imbibition dynamics in each sub-capillary of the modified interacting capillary bundle model. (a) Imbibition length versus time in each sub-capillary. (b) Proportion of pressure difference caused by gravity (Δp_g) to the capillary pressure difference (Δp_c) versus time in each sub-capillary. (c) Imbibition velocity (v) versus imbibition height of first sub-capillary (h_1). (d) Relative velocity difference compared with the imbibition velocity in the first sub-capillary versus the imbibition height of first sub-capillary. In all graphs, the solid lines represent the results considering gravity and the dashed lines indicate the results not considering gravity.

To illustrate at what position the corner film development becomes more pronounced, we further plot **Figure 13** (c) and (d). **Figure 13** (c) shows the imbibition velocity for different sub-capillaries versus the imbibition height of the main meniscus (h_1). **Figure 13** (d) shows the relative velocity difference of each corner sub-capillary compared with the first sub-capillary versus h_1. For illustration, we run the model with (solid lines) and without gravity (dashed lines). As can be seen, the development of the corner film depends on the difference in the imbibition velocity between the main meniscus and corner films. Without gravitational force, the imbibition

velocities in all sub-capillaries remain similar and the corner films develop very slowly. In the presence of gravity, when the imbibition height is small (h_1<2mm), the influence of gravity is negligible and the imbibition velocities of the sub-capillaries are similar. As a result, the imbibition height versus time in each sub-capillary almost collapses on the same line, as shown in **Figure 13** (a). With increasing imbibition height, the influence of gravity becomes more and more significant, especially for the first sub-capillary. When the imbibition height of main meniscus gets larger than 4mm, the relative difference between the smallest sub-capillary and the first sub-capillary (main meniscus) increases larger than 20%, resulting in a prominent development of corner film, as observed in **Figure 13** (a). Finally, when the main meniscus gradually approaches its equilibrium height after h_1>6mm, the velocities of the corner sub-capillaries diverge more and more from that of the main meniscus, yielding a much faster growth of corner film compared with the main meniscus. In summary, the arc meniscus in the corners develops with time, and this growth occurs more prominent as the main meniscus gets higher, as clearly shown in **Figure 10**. We note that when there is a high inlet flow resistance, even without gravitational force, the difference in the imbibition velocity between the main meniscus and corner films would also be significant, resulting in fast development of corner films.

4.4 Sensitivity analysis of different parameters on the imbibition dynamics in a square tube

In this section, both LBM simulation and the modified ICB model results are used to describe the imbibition dynamics with different fluid properties, in order to investigate the influences of different parameters on the imbibition dynamics, and to verify the accuracy and robustness of the modified ICB model under different conditions.

First, the influence of viscosity on the imbibition dynamics is investigated. As listed in **Table 1**, the viscosities of the liquid and gas phases in Case2 are twice of those in Case1 while the other parameters remain the same. The imbibition dynamics of the main meniscus in the center and of the arc meniscus in the corner for Case2 obtained by different methods are shown as red lines in **Figure 14**. In general, the prediction results of the modified ICB model agree with the LBM simulation results. With increasing fluid viscosity, the imbibition process becomes slower, as can be observed by comparing the black (Case1) and the red lines (Case2) in **Figure 15**, which shows the relationships between wetting fluid volume and time obtained by different

methods for different cases. As the conductance of each sub-capillary is inversely proportional to the fluid viscosity and the pressure difference ($\Delta p_c - \Delta p_g$) which drives the imbibition process is the same for different fluid viscosities, under the same imbibition height the imbibition rate is inversely proportional to the fluid viscosity accordingly. This can be observed by comparing the black and red lines in **Figure 16**, which shows the imbibition velocities of main (solid lines) and arc menisci (dashed lines) versus the imbibition height of main meniscus. Accordingly, for a certain imbibition height, the time range for Case2 is twice that for Case1. In addition, the prediction results of the modified ICB model match well with the LBM simulation results for the imbibition volume versus time.

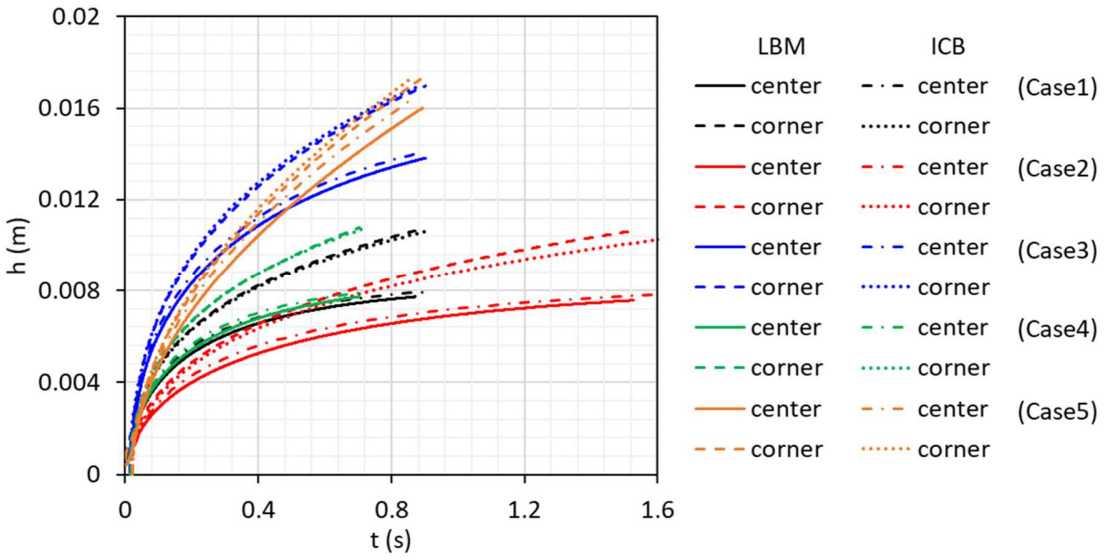

Figure 14. Imbibition heights of main and arc menisci versus time obtained by modified ICB and LBM for different viscosity (Case2), surface tension (Case3), wetting phase contact angle (Case4) and gravitational force (Case5).

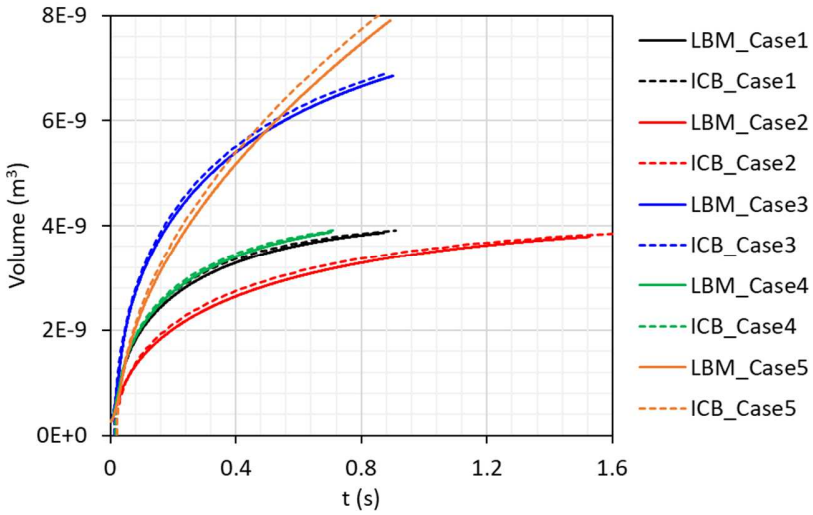

Figure 15. Relationship between wetting fluid volume and time obtained by modified ICB and LBM for different cases.

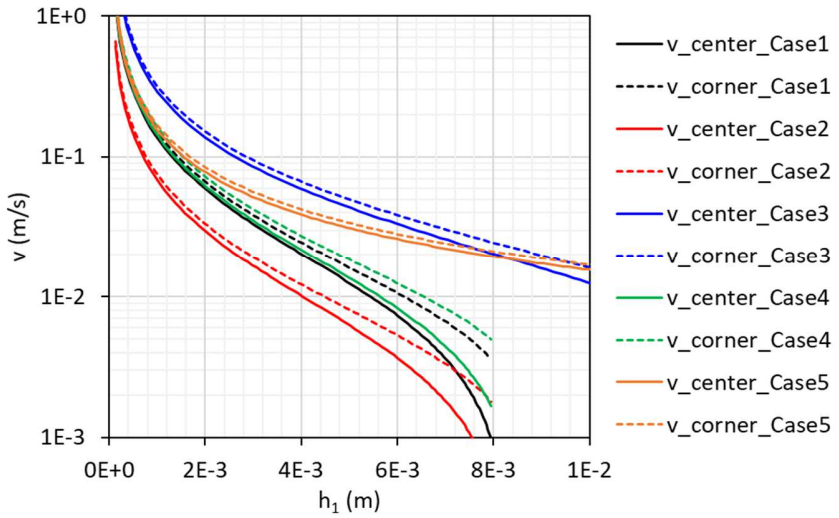

Figure 16. Imbibition velocity versus the imbibition height of the first sub-capillary for different cases.

The blue lines in **Figure 14**-**Figure 16** show the effect of surface tension on the imbibition dynamics. **Figure 14** shows that, in terms of imbibition heights, the prediction results of the modified ICB model match well with the LBM simulation results for Case3. **Figure 15** shows that, with increasing surface tension, the imbibition rate gets higher. For a certain imbibition height, the pressure difference caused by gravity (Δp_g) is the same for Case1 and

Case3. As the driving capillary pressure difference (Δp_c) is higher in Case3 because of the larger surface tension, the net pressure difference ($\Delta p_c - \Delta p_g$) which drives the imbibition process is larger in Case3, leading to a higher imbibition rate. Therefore, for the same imbibition height, the time range for Case3 is much smaller than that for Case1. In addition, for the same imbibition height, the influence of gravity is less important in Case3, resulting in smaller velocity differences between the main and arc meniscus, as shown in **Figure 16**. Accordingly, the imbibition height difference between the main and arc menisci becomes also smaller for the same imbibition height of main meniscus, as observed in **Figure 14**.

In Case4, the wetting phase contact angle is decreased to 12.6° while the other parameters remain the same as Case1. According to green lines shown in **Figure 14** and **Figure 15**, the prediction results of the modified ICB model match well with the LBM simulation results, for both imbibition height and volume. The contact angle influences both the driving capillary force and viscous force as it changes the shape of arc meniscus. With decreasing wetting phase contact angle, the driving capillary pressure difference (Δp_c) increases, and the cross section areas of the sub-capillaries in the corners also increase, resulting in an increase of the conductances of sub-capillaries in corners. Accordingly, the imbibition rate increases and the time range decreases for a certain imbibition height, as shown in **Figure 16**.

Finally, the influence of gravity is analyzed with Case5. As shown in section 4.3, and also the orange lines in **Figure 16**, for the case without gravitational force, the relative difference in imbibition velocity between the main and arc menisci is small and constant at different imbibition heights. Therefore, the difference in imbibition height between the main and arc menisci becomes much smaller when the gravitational force is not considered, as shown by the orange lines in **Figure 14**. According to **Figure 15**, at the early times of imbibition process, the influence of gravity is negligible and the imbibition volumes are similar for Case1 (black lines) and Case5 (orange lines). With progressing imbibition and increasing imbibition height, the imbibition volume in Case1 becomes much smaller than that in Case5 due to the influence of gravity.

According to above analysis, the main and arc menisci show different imbibition dynamics and time ranges with different fluid properties, which is caused by the different interactions between capillary, viscous and gravitational forces. The comparison results between

the modified ICB model and LBM simulations show that the modified ICB model can well describe the influences of different parameters on the imbibition dynamics in a square tube. In addition, the modified ICB model is very helpful to analyze the mechanisms during the imbibition process.

5 Discussion

We discuss the scaling law of spontaneous imbibition in a square tube. As stated in the introduction, the imbibition dynamics of the main meniscus in the square tube is similar to that in a circular tube due to the similarity in driving and resistance forces. In the viscous regime, the imbibition dynamics of the main meniscus considering gravity can be described by a more general formulation of equation (3):

$$-h-\frac{2\gamma}{\rho gRf\left(\theta\right)}\ln\left(1-\frac{\rho gRf\left(\theta\right)}{2\gamma}h\right)=\frac{b\rho gR^2}{\mu}t, \tag{19}$$

where $f\left(\theta\right)$ reflects the influence of wetting phase contact angle on the capillary pressure, b is a coefficient related to the calculation of viscous force. These two parameters are both dependent on the shape of the tube. For a circular tube, $f\left(\theta\right)=1/\cos\theta$, b=0.125 and equation (3) is recovered. For a square tube, $f\left(\theta\right)=2\left[\frac{\cos\theta-\sqrt{\left(\pi/4-\theta\right)+\sin\theta\cos\theta}}{\left(\theta-\pi/4\right)+\cos^2\theta-\sin\theta\cos\theta}\right]$ and b=0.140575.

We further normalize the imbibition height and time with the following characteristic length and time:

$$\begin{aligned} h^*&=\frac{h}{h_{eq}}=\frac{h}{2\gamma/\rho gRf\left(\theta\right)},\\ t^*&=\frac{t}{h_{eq}/u_g}=\frac{t}{2\gamma\mu/\left(\rho g\right)^2bR^3f\left(\theta\right)}, \end{aligned} \tag{20}$$

where h_{eq} is the equilibrium imbibition height balanced by capillary force and gravitational force. The equivalent height is inversely proportional to the radius R. $u_g=\rho gbR^2/\mu$ is the mean velocity in the tube when driven only by gravity. Then, equation (19) can be rewritten in the following simplified way:

$$-h^* - \ln\left(1-h^*\right) = t^* \tag{21}$$

Through expansion of the term $\ln\left(1-h^*\right)$ on the left-hand side of above equation, we get the following relationship:

$$\frac{h^{*2}}{2} + \frac{h^{*3}}{3} + \frac{h^{*4}}{4} + \ldots = t^* \tag{22}$$

We normalize the imbibition dynamics of both main and arc menisci based on equation (20) for Case1 to 4 and the results are shown in **Figure 17** (a). The imbibition dynamics in a circular tube used in the validation in section 3.2.2 is also plotted for comparison. As can be seen, the imbibition dynamics of main meniscus in the square tube and of the meniscus in the circular tube all collapse to the same line in the normalized form following equation (21) or (22). At early time of imbibition, h^* is very small and the influence of gravity can be neglected. Therefore, both the main and arc menisci develop as $\sim t^{*1/2}$. This is also reflected by equation (22). When h^* is very small, the first term dominates the left-hand side and all the higher order terms can be neglected, and equation (22) becomes $h^* = \sqrt{2t^*}$, which is in fact the Washburn equation not considering gravity. As time goes on, the higher order terms in equation (22) become more and more significant and the imbibition of main meniscus deviates from the scaling law of $\sim t^{*1/2}$. After t^*>1, the imbibition height of main meniscus gradually converges to the equilibrium height ($h^* \to 1$), while the arc meniscus develops in a slower rate to higher heights (h^* >1). In addition, we observe that the height of the arc meniscus for all cases also collapse to the same line for cases 1 to 3. These three cases have the same wetting phase contact angle, which determines the shape of arc meniscus and thus the resulting driving and resistance forces. A different wetting phase contact angle yields a different shape of arc meniscus and thus different imbibition dynamics. Accordingly, the dashed green line of arc meniscus for Case4 deviates slightly from the other lines.

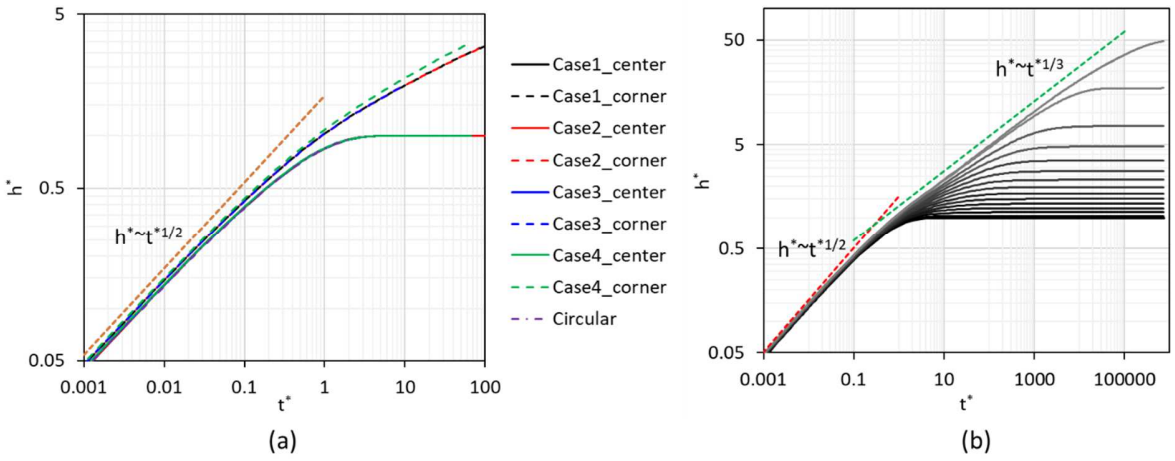

Figure 17. (a) Imbibition dynamics in square and circular tubes in normalized form. For the square tubes, cases 1 to 4 are plotted. (b) Imbibition dynamics in different sub-capillaries for Case1 in normalized form.

We further analyze the scaling law of the imbibition process for arc meniscus at late time after $t^*>1$. We set l_{min} to a small value ($l_{min}=0.02l_{max}$) and the number of sub-capillaries to a high value ($N_c=15$) in the decomposition process to get more detailed information on time behavior of the arc meniscus. The imbibition dynamics in different sub-capillaries are plotted in **Figure 17** (b) in normalized form. The bottom curve represents the main meniscus in the center and the top curve indicates the smallest sub-capillary in tip of the corner. From the center to corner, the equilibrium imbibition height gradually increases due to the smaller pore size (see equation 20). At early time, the tip of the corner develops as $\sim t^{*1/2}$, following the main meniscus. This is because the gravity can be neglected and the imbibition in each sub-capillary roughly follows the square root of time, as analyzed above. The main meniscus has the highest imbibition rate due to the largest pore size and corresponding smallest flow resistance. As the imbibition of arc meniscus is driven by the capillary pressure difference between main and arc menisci, the fast invading main meniscus pushes the arc meniscus to develop in a similar rate. While at late time ($t^*>1$), the main meniscus nearly stops at equilibrium height and the tip of the corner develops in a slower rate as $\sim t^{*1/3}$ for some time, which has also been observed in experiments (Ponomarenko et al., 2011). The slower imbibition rate is mainly because of the smaller size of sub-capillaries and corresponding larger flow resistance. Finally, the capillary in the tip of the corner will also deviate from the scaling law of $\sim t^{*1/3}$ and reach an equilibrium height, which is determined by the l_{min} set in the modified ICB model. With a smaller l_{min}, the scaling law of

$\propto t^{*1/3}$ for the tip-corner capillary persists for a longer period as the modified ICB model covers a broader range of the arc meniscus.

6 Conclusion

In this paper, a modified interacting capillary bundle model is developed to describe the imbibition dynamics of a liquid-gas system in a square tube with corner films. The square tube is decomposed into several sub-capillaries and fluid can flow laterally between two connecting sub-capillaries without flow resistance. The local capillary pressure in each sub-capillary is determined based on the shape of meniscus and the flow resistance is upscaled from single-phase lattice Boltzmann simulation results. The imbibition dynamics in a square tube with different fluid properties is calculated with both the modified ICB model and a color-gradient lattice Boltzmann method. The predictions of the modified ICB model match well with the LBM simulation results under different conditions, in terms of both the imbibition volume and imbibition heights of main and arc meniscus, demonstrating the accuracy and robustness of the modified ICB model to describe the imbibition dynamics in a square tube. It should be mentioned that the original ICB model can only predicts well the imbibition dynamics of main meniscus but significantly overestimates the imbibition rate of arc meniscus as its lack of fidelity to geometry prevents it from accurately describing the relationship between driving and resistance forces of arc meniscus.

In addition, the influences of different parameters on the imbibition dynamics and the underlying mechanisms are analyzed in detail with the help of the modified ICB model. The fluid viscosity affects the imbibition process through changing the conductance of each sub-capillary. The imbibition rate is inversely proportional to the fluid viscosity. A higher surface tension results in a larger driving capillary force, which results in a faster imbibition rate. In addition, the influence of gravity becomes less important for a certain imbibition height with the higher surface tension. With decreasing wetting phase contact angle, both the driving capillary force and the conductance of corner film increase, resulting in a higher imbibition rate. If gravity is not considered, the imbibition rate becomes much faster. In addition, the relative imbibition velocity differences between the main and arc menisci are small and remain constant at different imbibition heights, resulting in a smaller difference of imbibition length between the main and arc menisci.

Finally, the scaling law of imbibition dynamics for both the main and arc menisci is discussed. A universal scaling law describing the imbibition dynamics of main meniscus is developed, which applies to different shapes of tubes. At early time, the arc meniscus develops as $\sim t^{*1/2}$, following the imbibition of main meniscus. At later time when the main meniscus reaches its equilibrium height, the tip of the corner develops according to $\sim t^{*1/3}$, which agrees with some experimental observations.

In summary, the modified interacting capillary model is simple and accurate to describe the imbibition dynamics in a square tube with corner films. In addition, it is very helpful to understand the mechanisms of the imbibition process and can be easily extended to other geometries. However, the developed model experiences some limitations. First, it only applies to gas-liquid systems as the viscous dissipation in the non-wetting gas phase is neglected. Second, the model assumes the pores to be straight tubes and cannot directly be used in more complex porous media. Both these limitations will be addressed in our future work.

Acknowledgements and Data

This work was supported by the Swiss National Science Foundation (Project No. 175793) and the Swiss National Supercomputing Centre (Project No. s823). Q.K. acknowledges the support from LANL's LDRD Program. The data associated with this paper are made available from https://www.research-collection.ethz.ch/handle/20.500.11850/447959.

References

Akai, T., Bijeljic, B., & Blunt, M. J. (2018). Wetting boundary condition for the color-gradient lattice Boltzmann method: Validation with analytical and experimental data. *Advances in Water Resources*, *116*(November 2017), 56–66. https://doi.org/10.1016/j.advwatres.2018.03.014

Arunkumar, T., Wang, J., & Denkenberger, D. (2020). Capillary flow-driven efficient nanomaterials for seawater desalination: Review of classifications, challenges, and future perspectives. *Renewable and Sustainable Energy Reviews*, 110547.

Bosanquet, C. H. (1923). LV. On the flow of liquids into capillary tubes. *The London, Edinburgh, and Dublin Philosophical Magazine and Journal of Science*, *45*(267), 525–531.

Cai, J., Perfect, E., Cheng, C.-L., & Hu, X. (2014). Generalized modeling of spontaneous imbibition based on Hagen–Poiseuille flow in tortuous capillaries with variably shaped apertures. *Langmuir*, *30*(18), 5142–5151.

Chauvet, F., Duru, P., Geoffroy, S., & Prat, M. (2009). Three periods of drying of a single square capillary tube. *Physical Review Letters*, *103*(12), 124502.

Chen, L., Kang, Q., Mu, Y., He, Y.-L., & Tao, W.-Q. (2014). A critical review of the pseudopotential multiphase lattice Boltzmann model: Methods and applications. *INTERNATIONAL JOURNAL OF HEAT AND MASS TRANSFER*, *76*, 210–236. https://doi.org/10.1016/j.ijheatmasstransfer.2014.04.032

Chen, Y., Valocchi, A. J., Kang, Q., & Viswanathan, H. S. (2019). Inertial Effects During the Process of Supercritical CO2 Displacing Brine in a Sandstone: Lattice Boltzmann Simulations Based on the Continuum□Surface□Force and Geometrical Wetting Models. *Water Resources Research*, *55*(12), 11144–11165.

Das, S., Waghmare, P. R., & Mitra, S. K. (2012). Early regimes of capillary filling. *Physical Review E*, *86*(6), 67301.

Dong, M, & Chatzis, I. (1995). The imbibition and flow of a wetting liquid along the corners of a square capillary tube. *Journal of Colloid and Interface Science*, *172*(2), 278–288.

Dong, Mingzhe, & Zhou, J. (1998). Characterization of waterflood saturation profile histories by the 'complete'capillary number. *Transport in Porous Media*, *31*(2), 213–237.

Dong, Mingzhe, Dullien, F. A. L., Dai, L., & Li, D. (2005). Immiscible displacement in the interacting capillary bundle model part I. Development of interacting capillary bundle model. *Transport in Porous Media*, *59*(1), 1–18.

Fries, N., & Dreyer, M. (2008a). An analytic solution of capillary rise restrained by gravity. *Journal of Colloid and Interface Science*, *320*(1), 259–263.

Fries, N., & Dreyer, M. (2008b). The transition from inertial to viscous flow in capillary rise. *Journal of Colloid and Interface Science*, *327*(1), 125–128.

De Gennes, P.-G., Brochard-Wyart, F., & Quéré, D. (2013). *Capillarity and wetting phenomena: drops, bubbles, pearls, waves*. Springer Science & Business Media.

Golparvar, A., Zhou, Y., Wu, K., Ma, J., & Yu, Z. (2018). A comprehensive review of pore scale modeling methodologies for multiphase flow in porous media. *Advances in Geo-Energy Research*, *2*(4), 418–440.

Groot, R. D., & Warren, P. B. (1997). Dissipative particle dynamics: Bridging the gap between atomistic and mesoscopic simulation. *The Journal of Chemical Physics*, *107*(11), 4423–4435.

Gurumurthy, V. T., Rettenmaier, D., Roisman, I. V, Tropea, C., & Garoff, S. (2018). Computations of spontaneous rise of a rivulet in a corner of a vertical square capillary. *Colloids and Surfaces A: Physicochemical and Engineering Aspects*, *544*, 118–126.

Huang, H., Huang, J.-J., & Lu, X.-Y. (2014). Study of immiscible displacements in porous media using a color-gradient-based multiphase lattice Boltzmann method. *COMPUTERS & FLUIDS*, *93*, 164–172. https://doi.org/10.1016/j.compfluid.2014.01.025

Huang, H., Sukop, M., & Lu, X. (2015). *Multiphase lattice Boltzmann methods: Theory and application*. John Wiley & Sons.

Kao, C. S., & Hunt, J. R. (1996). Prediction of wetting front movement during one□dimensional infiltration into soils. *Water Resources Research*, *32*(1), 55–64.

Lal, S., Prat, M., Plamondon, M., Poulikakos, L., Partl, M. N., Derome, D., & Carmeliet, J. (2019). A cluster-based pore network model of drying with corner liquid films, with application to a macroporous material. *International Journal of Heat and Mass Transfer*, *140*, 620–633.

Laurindo, J. B., & Prat, M. (1998). Numerical and experimental network study of evaporation in capillary porous media. Drying rates. *Chemical Engineering Science*, *53*(12), 2257–2269.

Leclaire, S., Parmigiani, A., Malaspinas, O., Chopard, B., & Latt, J. (2017). Generalized three-dimensional lattice Boltzmann color-gradient method for immiscible two-phase pore-scale imbibition and drainage in porous media. *Physical Review E*, *95*(3), 33306.

Li, C., Singh, H., & Cai, J. (2019). Spontaneous imbibition in shale: A review of recent advances. *Capillarity*, *2*(2), 17–32.

Li, S., Dong, M., & Luo, P. (2017). A crossflow model for an interacting capillary bundle:

Development and application for waterflooding in tight oil reservoirs. *Chemical Engineering Science*, *164*, 133–147.

Liu, H., Valocchi, A. J., & Kang, Q. (2012). Three-dimensional lattice Boltzmann model for immiscible two-phase flow simulations. *Physical Review E*, *85*(4), 46309.

Liu, H., Valocchi, A. J., Werth, C., Kang, Q., & Oostrom, M. (2014). Pore-scale simulation of liquid CO2 displacement of water using a two-phase lattice Boltzmann model. *Advances in Water Resources*, *73*, 144–158.

Liu, H., Zhang, Y., & Valocchi, A. J. (2015). Lattice Boltzmann simulation of immiscible fluid displacement in porous media: Homogeneous versus heterogeneous pore network. *Physics of Fluids*, *27*(5), 52103.

Liu, H., Kang, Q., Leonardi, C. R., Schmieschek, S., Narváez, A., Jones, B. D., et al. (2016). Multiphase lattice Boltzmann simulations for porous media applications. *Computational Geosciences*, *20*(4), 777–805.

Liu, Z., He, X., Han, J., Zhang, X., Li, F., Li, A., et al. (2018). Liquid wicking behavior in paper-like materials: mathematical models and their emerging biomedical applications. *Microfluidics and Nanofluidics*, *22*(11), 132.

Meng, Q., Liu, H., & Wang, J. (2017). A critical review on fundamental mechanisms of spontaneous imbibition and the impact of boundary condition, fluid viscosity and wettability. *Adv. Geo-Energy Res*, *1*(1), 1–17.

Morrow, N. R., & Mason, G. (2001). Recovery of oil by spontaneous imbibition. *Current Opinion in Colloid & Interface Science*, *6*(4), 321–337.

Parada, M., Derome, D., Rossi, R. M., & Carmeliet, J. (2017). A review on advanced imaging technologies for the quantification of wicking in textiles. *Textile Research Journal*, *87*(1), 110–132.

Parada, M., Vontobel, P., Rossi, R. M., Derome, D., & Carmeliet, J. (2017). Dynamic wicking process in textiles. *Transport in Porous Media*, *119*(3), 611–632.

Perwuelz, A., Mondon, P., & Caze, C. (2000). Experimental study of capillary flow in yarns. *Textile Research Journal*, *70*(4), 333–339.

Ponomarenko, A., Quéré, D., & Clanet, C. (2011). A universal law for capillary rise in corners. *Journal of Fluid Mechanics*.

Qin, C.-Z., & van Brummelen, H. (2019). A dynamic pore-network model for spontaneous imbibition in porous media. *Advances in Water Resources*, *133*, 103420.

Qin, F., Mazloomi Moqaddam, A., Kang, Q., Derome, D., & Carmeliet, J. (2018). Entropic multiple-relaxation-time multirange pseudopotential lattice Boltzmann model for two-phase flow. *Physics of Fluids*, *30*(3), 32104.

Qin, F., Del Carro, L., Moqaddam, A. M., Kang, Q., Brunschwiler, T., Derome, D., & Carmeliet, J. (2019). Study of non-isothermal liquid evaporation in synthetic micro-pore structures with hybrid lattice Boltzmann model. *Journal of Fluid Mechanics*, *866*, 33–60.

Qin, F., Su, M., Zhao, J., Moqaddam, A. M., Del Carro, L., Brunschwiler, T., et al. (2020). Controlled 3D nanoparticle deposition by drying of colloidal suspension in designed thin micro-porous architectures. *International Journal of Heat and Mass Transfer*, *158*, 120000.

Raiskinmäki, P., Shakib-Manesh, A., Jäsberg, A., Koponen, A., Merikoski, J., & Timonen, J. (2002). Lattice-Boltzmann simulation of capillary rise dynamics. *Journal of Statistical Physics*, *107*(1–2), 143–158.

Schmid, K. S., & Geiger, S. (2012). Universal scaling of spontaneous imbibition for water□wet systems. *Water Resources Research*, *48*(3).

Son, S., Chen, L., Kang, Q., Derome, D., & Carmeliet, J. (2016). Contact angle effects on pore and corner arc menisci in polygonal capillary tubes studied with the pseudopotential multiphase lattice Boltzmann model. *Computation*, *4*(1), 12.

Sukop, M. (2006). DT Thorne, Jr. Lattice Boltzmann Modeling Lattice Boltzmann Modeling.

Tang, L.-H., & Tang, Y. (1994). Capillary rise in tubes with sharp grooves. *Journal de Physique II*, *4*(5), 881–890.

Wang, J., Dong, M., & Yao, J. (2012). Calculation of relative permeability in reservoir engineering using an interacting triangular tube bundle model. *Particuology*, *10*(6), 710–721.

Washburn, E. W. (1921). The dynamics of capillary flow. *Physical Review*, *17*(3), 273.

Weislogel, M. M. (2012). Compound capillary rise. *Journal of Fluid Mechanics*, *709*, 622–647.

Wu, R., Zhang, T., Ye, C., Zhao, C. Y., Tsotsas, E., & Kharaghani, A. (2020). Pore network model of evaporation in porous media with continuous and discontinuous corner films. *Physical Review Fluids*, *5*(1), 14307.

Xu, Z., Liu, H., & Valocchi, A. J. (2017). Lattice B oltzmann simulation of immiscible two□ phase flow with capillary valve effect in porous media. *Water Resources Research*, *53*(5), 3770–3790.

Yang, Q., Yao, J., Huang, Z., Zhu, G., Liu, L., & Song, W. (2020). Pore-scale investigation of petro-physical fluid behaviours based on multiphase SPH method. *Journal of Petroleum Science and Engineering*, 107238.

Yang, Y., Yao, J., Wang, C., Gao, Y., Zhang, Q., An, S., & Song, W. (2015). New pore space characterization method of shale matrix formation by considering organic and inorganic pores. *Journal of Natural Gas Science and Engineering*, *27*, 496–503.

Yang, Y., Yang, H., Tao, L., Yao, J., Wang, W., Zhang, K., & Luquot, L. (2019). Microscopic determination of remaining oil distribution in sandstones with different permeability scales using computed tomography scanning. *Journal of Energy Resources Technology*, *141*(9).

Yu, T., Zhou, J., & Doi, M. (2018). Capillary imbibition in a square tube. *Soft Matter*, *14*(45), 9263–9270.

Zhang, L., Xu, C., Guo, Y., Zhu, G., Cai, S., Wang, X., et al. (n.d.). The Effect of Surface Roughness on Immiscible Displacement Using Pore Scale Simulation. *Transport in Porous Media*, 1–13.

Zhao, B., MacMinn, C. W., Primkulov, B. K., Chen, Y., Valocchi, A. J., Zhao, J., et al. (2019). Comprehensive comparison of pore-scale models for multiphase flow in porous media. *Proceedings of the National Academy of Sciences*, 201901619.

Zhao, J., Kang, Q., Yao, J., Viswanathan, H., Pawar, R., Zhang, L., & Sun, H. (2018). The Effect of Wettability Heterogeneity on Relative Permeability of Two-Phase Flow in Porous Media: A Lattice Boltzmann Study. *Water Resources Research*, *54*(2).

Zhao, Jianlin, Qin, F., Derome, D., Kang, Q., & Carmeliet, J. (2020). Improved pore network

models to simulate single-phase flow in porous media by coupling with lattice Boltzmann method. *Advances in Water Resources*, *145*, 103738.

Zhao, Jianlin, Qin, F., Derome, D., & Carmeliet, J. (2020). Simulation of Quasi-static Drainage Displacement in Porous Media on Pore-scale: Coupling Lattice Boltzmann Method and Pore Network Model. *Journal of Hydrology*, 125080.

Zhu, G., Chen, H., Yao, J., & Sun, S. (2019). Efficient energy-stable schemes for the hydrodynamics coupled phase-field model. *Applied Mathematical Modelling*, *70*, 82–108.

Zhu, G., Kou, J., Yao, B., Wu, Y., Yao, J., & Sun, S. (2019). Thermodynamically consistent modelling of two-phase flows with moving contact line and soluble surfactants. *Journal of Fluid Mechanics*, *879*, 327–359.